A Numerical Study of the Drag on a Sphere at Low and Intermediate Reynolds Numbers

B. P. LE CLAIR AND A. E. HAMIELEC

Chemical Engineering Dept., McMaster University, Hamilton, Canada

AND H. R. PRUPPACHER

Dept. of Meteorology, University of California, Los Angeles

(Manuscript received 22 August 1969, in revised form 9 December 1969)

ABSTRACT

Accurate solutions of the steady-state Navier-Stokes equations of motion have been obtained by means of a numerical method to determine the hydrodynamic drag on a rigid sphere falling at its terminal velocity in an unbounded fluid. The calculations were carried out for Reynolds numbers between 0.01 and 400. The numerical solutions were compared with the theoretical results of Stokes, Oseen, Goldstein, Proudman and Pearson, Jenson, Rimon and Cheng, and Carrier, and with the recent experimental data of Maxworthy, and Pruppacher and Steinberger. At the lowest Reynolds numbers the numerical solutions show closest agreement with the theory of Proudman and Pearson and at intermediate Reynolds numbers with the semi-theoretical relationship proposed by Carrier. At higher Reynolds numbers our present results agree well with the calculations of Hamielec *et al.* for Reynolds numbers of 40 and 100 and with the numerical results of Rimon and Cheng; they depart, however, significantly from the results of Jenson. Over the whole Reynolds number interval 0.01–400 our numerical results are in close agreement with the experimental data of Pruppacher, Pruppacher and Steinberger, and Beard and Pruppacher. It is concluded that our numerical study is unique in that it is able to predict theoretically accurate values for the drag on a sphere over a wide Reynolds number interval. The present study also confirms the findings of Maxworthy, and Pruppacher and Steinberger, that as the Reynolds number approaches zero the drag on a sphere approaches zero via the Oseen drag rather than via the Stokes drag. The significance of the present results to cloud physics is pointed out.

1. Introduction

A large number of experimental and theoretical investigations on the drag force on a rigid sphere falling at its terminal velocity in a viscous medium has been reported in the literature. Recently, Maxworthy (1965) and Pruppacher and Steinberger (1968) showed that if the actual drag D on a sphere is nondimensionalized by the Stokes drag D_s and the quantity $(D/D_s)-1$ is plotted as a function of the Reynolds number, large differences between the various experimental and theoretical results are revealed. In an attempt to resolve these differences new experiments were carried out by Pruppacher (1969, unpublished) for Reynolds number $0.1 \leq N_{Re} \leq 300$. These results agree well[1] with those carried out by Pruppacher and Steinberger for $0.001 \leq N_{Re} \leq 10$. Further confirmation of these results was given recently by Beard and Pruppacher (1969) who by means of a wind tunnel experimentally determined the drag on water drops falling at terminal velocity in air and having Reynolds numbers $0.1 \leq N_{Re} \leq 200$. The close agreement between these new results and those for rigid spheres of Pruppacher and Steinberger and Pruppacher suggests the conclusion that as far as the hydrodynamic drag is concerned water drops with Reynolds numbers $N_{Re} \leq 200$ (i.e., radii less than about 450 μ) behave as solid rather than liquid spheres. Recent studies in the field of cloud physics have repeatedly stressed the importance of an exact knowledge of how the hydrodynamic drag on water drops affects their physical behavior. Beard and Pruppacher showed, for instance, that in the Reynolds number interval $0.1 \leq N_{Re} \leq 200$ the quantity $(D/D_s)-1$ can be well approximated by empirical relations of the from $(D/D_s)-1=\alpha N_{Re}^{\beta}$ (where α and β are constants). These relations allow an easy and accurate determination of the terminal velocity of cloud drops for all conditions in the atmosphere. The drag force acting on a sphere also gives information on the physical characteristics of the flow field of the fluid streaming past it. An accurate knowledge of the flow field past falling spheres in turn helps to provide an accurate description of the interaction forces between two spheres falling in close proximity behind each other, a problem which enters importantly in computing collision efficiencies of falling cloud drops. For computing such collision efficiencies, Langmuir (1948) assumed potential

[1] At $N_{Re} < 1$ the most recent values for $(D/D_s)-1$ (Pruppacher, 1969, unpublished) tended to be somewhat higher than those of Pruppacher and Steinberger. The scatter in the values seems to be caused by the progressively increasing effect of the error involved in determining the viscosity of the medium.

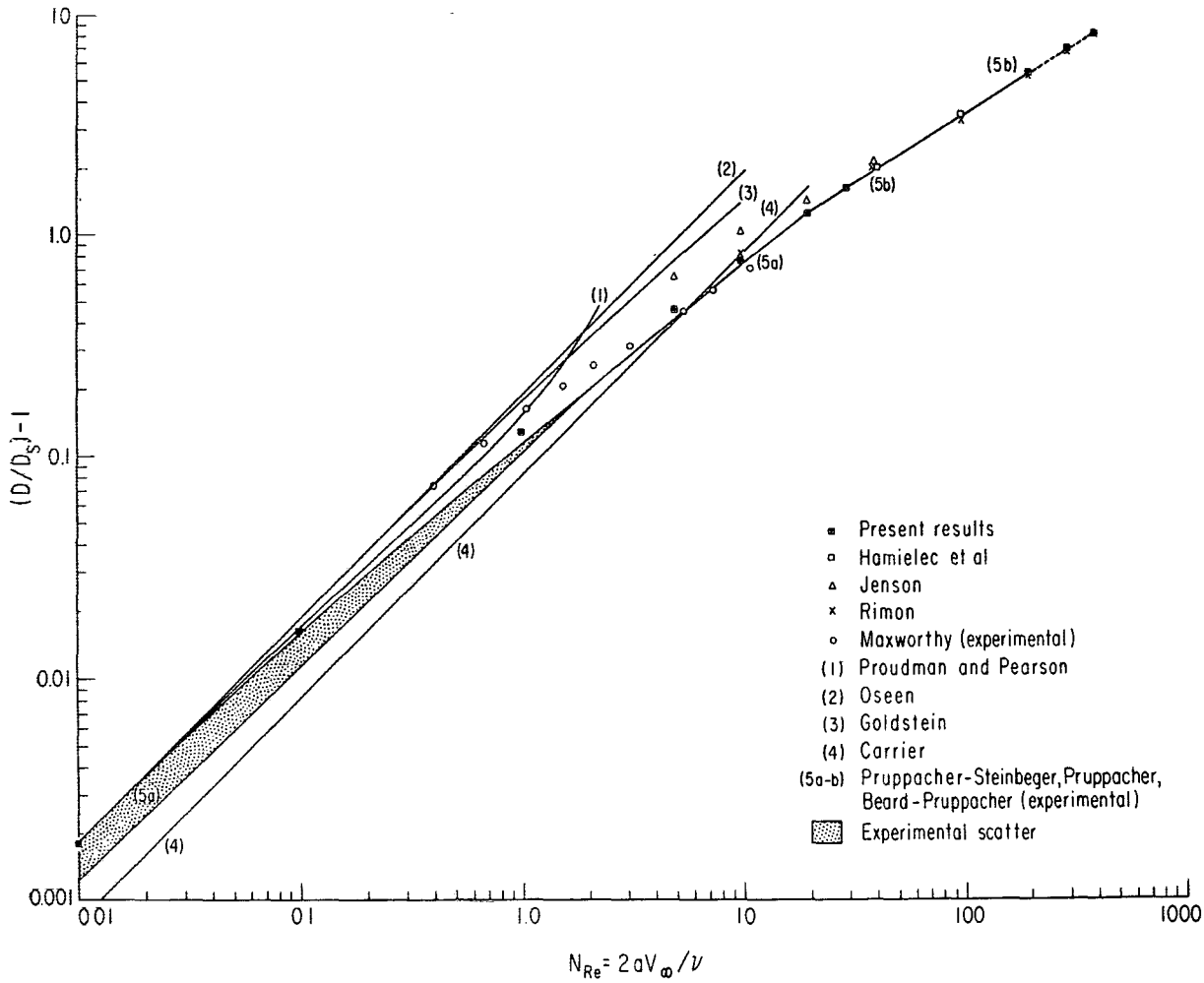

FIG. 1. Variation of the quantity $(D/D_s)-1$ with Reynolds number (comparison of theory and experiment).

flow to describe the flow field around drops with high Reynolds numbers and Stokes flow around drops with small Reynolds numbers. Pearcey and Hill (1957) chose Goldstein's (1929) solution for Oseen flow past a sphere. Shafrir and Neiburger (1963) employed Stokes flow for drops with $N_{Re} \leq 0.44$ (corresponding to drops of $a \leq 30$ μ in an atmosphere of 900 mb and 0C) and a modified form of Jenson's (1959) numerical solution to the complete steady-state Navier-Stokes equations for drops with $N_{Re} > 0.44$. Plumlee and Semonin (1965) used the method of matched asymptotic expansions developed by Proudman and Pearson (1957) to describe the flow field around a sphere. Klett (1969) calculated collision efficiencies of water drops of Reynolds numbers up to 4.16 ($a=70$ μ) based upon Carrier's (1953) modified Oseen flow fields. The Stokes flow model was used by Hocking (1959) and later in an improved fashion by Davis (1966) and Davis and Sartor (1967) to calculate the collision efficiency of drops of radii $a \leq 30$ μ, using a solution to the Stokesian hydrodynamic equations that fully allowed for the presence of the two spheres. The range of application of the Stokes flow model has recently been challenged by Maxworthy (1965), Pruppacher and Steinberger (1968), and by Steinberger *et al.* (1968). From an experimental determination of the drag on a single sphere falling in a viscous medium, Maxworthy, and Pruppacher and Steinberger, concluded that as N_{Re} approaches zero the drag approaches zero via the Oseen drag rather than via the Stokes drag. This finding may be interpreted to mean that the flow about a sphere is, strictly speaking, only symmetric with respect to a plane perpendicular to the flow at $N_{Re}=0$ and asymmetric at all $N_{Re}>0$. This concept recieved considerable support by the experiments of Stienberger *et al.* who determined the velocities, accelerations and drag forces experienced by two equal spheres falling along their line of centers in a viscous fluid at Reynolds numbers between 0.216 and 0.060. These authors found that even at the lowest Reynolds number investigated both spheres continually accelerated as they fell, and the upper sphere fell faster and accelerated more than the lower one, a result which must be interpreted as being

due entirely to non-Stokes behavior of the fluid. These results suggest that the deviation of the actual flow from Stokes flow around a sphere may, even at small Reynolds numbers, have significant effects in the sense that even small inertial accelerations in the fluid are able to cause a significant differential rate of fall between two spheres, affecting their relative trajectories and thus their collision efficiency. In particular, these effects may be important to the interaction of almost equal size spheres.

In the past, various theories have been advanced to determine the hydrodynamic drag on a sphere falling in a viscous medium. The results of these theories are compared with the experiments by Maxworthy, Pruppacher, and Pruppacher and Steinberger in Fig. 1 where $(D/D_s)-1$ has been plotted as a function of N_{Re} on a log-log scale. It is seen from this figure that at $N_{Re}>1$ the theories of Oseen (1927), Goldstein, and Proudman and Pearson deviate progressively from the experimental results. Recently, Chester and Breach (1969) extended the Proudman and Pearson theory to higher order terms in the hope of increasing the range of applicability of this theory. However, they had to conclude that the additional terms in the expansion not only did not improve the agreement with the experiment but on the contrary caused the disagreement to be even more pronounced. A considerable improvement over Oseen's theory was achieved by the semi-empirical considerations of Carrier (1953). Fig. 1 shows, at least for $2\leq N_{Re}\leq 20$, that Carrier's theory is a fair approximation to the experiment. In the range of higher Reynolds numbers, computations of the drag on a sphere were carried out by Jenson (1959), Hamielec *et al.* (1967), and Rimon and Cheng (1969) who solved the Navier-Stokes equations by numerical techniques. It is seen from Fig. 1 that Jenson considerably overestimates the drag while Hamielec *et al.*, and Rimon and Cheng, are in excellent agreement with the experiment. No numerical calculations of the drag on a sphere have so far been carried out for low Reynolds numbers. Part of the reason for this fact is that at low Reynolds numbers considerable difficulties in the numerical calculations arise due to step size and, particularly, wall effect errors. Hamielec *et al.* investigated these effects in detail and showed that wall effects may be a significant source of error in the drag if $N_{Re}<10$. Encouraged by the excellent agreement between the numerical results of Hamielec *et al.* and the experiment at higher Reynolds numbers, we extended the numerical computations of the drag force to the regime of lower Reynolds numbers. It was hoped that these numerical computations would provide values for the drag force on a sphere at low Reynolds numbers which would be in substantially better agreement with the experiment than those derived from analytical solutions to the Navier-Stokes equations of motion. Such computations would provide realistic flow fields past a sphere, and thus a clearer understanding of the air flow past cloud drops and the mode of interaction between them.

2. Present formulation

In the present investigation, values for the drag on a sphere falling in a viscous medium at its terminal velocity have been computed by solving the Navier-Stokes equation numerically with the aid of a digital computer. For this purpose a finite difference technique, described in detail by Hamielec *et al.*, was employed. Briefly, using all quanitities in their nondimensionalized form[2] the complete, steady-state Navier-Stokes equations for viscous, incompressible, axisymmetric flow in terms of the stream function in spherical coordinates can be written as

$$\frac{N_{Re}}{2}\left[\frac{\partial\psi}{\partial r}\frac{\partial}{\partial\theta}\left(\frac{E^2\psi}{r^2\sin^2\theta}\right)-\frac{\partial\psi}{\partial\theta}\frac{\partial}{\partial r}\left(\frac{E^2\psi}{r^2\sin^2\theta}\right)\right]\sin\theta=E^4\psi, \quad (1)$$

where

$$E^2=\frac{\partial^2}{\partial r^2}+\frac{\sin\theta}{r^2}\frac{\partial}{\partial\theta}\left(\frac{1}{\sin\theta}\frac{\partial}{\partial\theta}\right).$$

Eq. (1) may be split into two simultaneous second-order equations by introducing the vorticity in the form

$$E^2\psi=\zeta r\sin\theta. \quad (2)$$

Eq. (1) then becomes

$$\frac{N_{Re}}{2}\left[\frac{\partial\psi}{\partial r}\frac{\partial}{\partial\theta}\left(\frac{\zeta}{r\sin\theta}\right)-\frac{\partial\psi}{\partial\theta}\frac{\partial}{\partial r}\left(\frac{\zeta}{r\sin\theta}\right)\right]\sin\theta$$
$$=E^2(\zeta r\sin\theta). \quad (3)$$

The velocity components are related to the stream function by

$$v_\theta=\left(\frac{1}{r\sin\theta}\right)\frac{\partial\psi}{\partial r}, \quad v_r=-\left(\frac{1}{r^2\sin\theta}\right)\frac{\partial\psi}{\partial\theta}. \quad (4a,b)$$

The boundary conditions used for solving (2) and (3) are given by Eqs. (5):

Along the axis of symmetry

$$\theta=0^\circ \text{ and } \theta=180^\circ,\ \psi=0,\ \zeta=0. \quad (5a)$$

On the sphere surface

$$r=1,\quad \psi=0,\quad \zeta=\frac{E^2\psi}{\sin\theta}. \quad (5b)$$

On the boundary remote from the surface of the sphere and concentric with the sphere there is undisturbed parallel flow

$$r=r_\infty,\quad \psi=\tfrac{1}{2}r_\infty^2\sin^2\theta,\quad \zeta=0. \quad (5c)$$

[2] See Appendix for list of symbols.

TABLE 1. Effect of computational parameters on drag coefficient and stagnation pressure.

N_{Re}	A	B (deg.)	r_∞	V	W	C_{DP} (r_∞)	C_{DF} (r_∞)	C_D (r_∞)	P_o	P_π
0.01	0.05	3	90	1.0	1.0	811.096	1635.598	2446.695	617.933	-599.700
0.01	0.05	3	365	1.0	1.0	799.993	1613.206	2413.199	609.693	-591.307
0.01	0.05	3	1000	1.0	1.0	798.483	1610.186	2408.669	608.583	-590.151
0.1	0.05	3	90	1.0	1.0	81.652	164.572	246.224	63.041	- 59.541
0.1	0.05	3	365	1.0	1.0	81.025	163.382	244.407	62.640	- 59.000
0.1	0.05	3	1000	1.0	1.0	81.056	163.445	244.501	62.664	- 59.023
1.0	0.05	3	150	1.0	0.5	9.114	18.281	27.394	7.797	- 5.898
1.0	0.1	6	221	0.5	0.5	8.975	18.456	27.432	7.995	- 5.528
1.0	0.05	3	1000	1.0	0.1	9.086	18.289	27.375	7.810	- 5.843
5.0	0.05	3	90	1.0	0.25	2.444	4.677	7.121	2.601	- 1.163
10.0	0.05	3	90	1.0	0.1	1.536	2.801	4.337	1.869	- 0.606
20.0	0.05	3	90	1.0	0.1	1.017	1.719	2.736	1.469	- 0.326
30.0	0.05	3	90	1.0	0.05	0.818	1.307	2.126	1.326	- 0.237
100.0	0.025	3	12	1.0	0.1	0.507	0.590	1.096	1.106	- 0.163
200.0	0.025	3	12	1.0	0.1	0.400	0.372	0.772	1.055	- 0.143
300.0	0.025	3	12	1.0	0.07	0.350	0.283	0.632	1.037	- 0.123
400.0	0.025	3	12	1.0	0.02	0.320	0.232	0.552	1.028	- 0.117

Eqs. (2) and (3) together with the boundary conditions (5) were solved simultaneously by the finite difference technique discussed by Hamielec *et al.*, and values for the drag on a sphere at Reynolds numbers between 0.01 and 400 calculated using an electronic digital computer. The solutions were considered to have converged when $\psi^{n+1}-\psi^n<10^{-5}$ and $\zeta^{n+1}-\zeta^n<10^{-5}$ at all mesh points.

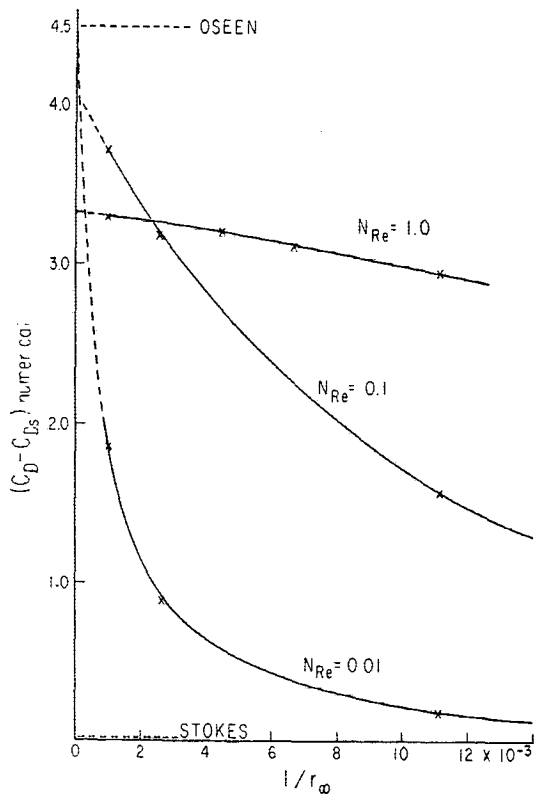

FIG. 2. Variation of numerically computed values for C_D-C_{Ds} as a function of distance to outer boundary.

The step sizes and the position of the outer boundary $r=r_\infty$ were varied in order to test the accuracy of the solutions. The result of these tests are shown in Table 1. In simulating an unbounded fluid the position of the outer boundary is limited to about 1000 sphere radii by requirements for core storage and, particularly, computation time. The errors resulting from the position of the outer boundary and those resulting from finite step size were estimated from comparisons between the analytical and the numerical solutions to the Navier-Stokes equation. For Stokes flow the Navier-Stokes equation of motion reduces to the linear form

$$E^4\psi=0. \tag{6}$$

This equation, together with the same boundary conditions as those for the nonlinear equation, was solved numerically. Alternatively, (6) can be solved analytically, where the stream function can be expressed as

$$\psi=[(A'/r)+B'r+C'r^2+D'r^4]\sin^2\theta. \tag{7}$$

The constants A', B', C' and D' in (7) were found by Hamielec *et al.*, satisfying the same boundary conditions as those for the numerical solution, and are given as a function of r_∞ by

$$\left.\begin{aligned} A'&=\frac{r_\infty^3-(5/2)r_\infty^6}{2-10r_\infty^3+18r_\infty^5-10r_\infty^6}\\ B'&=\frac{(15/2)r_\infty^6}{2-10r_\infty^3+18r_\infty^5-10r_\infty^6}\\ C'&=\frac{-(5/2)r_\infty^3-5r_\infty^6}{2-10r_\infty^3+18r_\infty^5-10r_\infty^6}\\ D'&=\frac{(3/2)r_\infty^3}{2-10r_\infty^3+18r_\infty^5-10r_\infty^6} \end{aligned}\right\}. \tag{8}$$

TABLE 2. Effect of boundary on computation of C_D.

N_{Re}	r_∞	C_D from analytical solution. Equ. (9)	C_D from numerical solution. Equ. (6)	C_D from numerical solution. Equ. (2) & (3)	C_D corrected for unbounded fluid
0.01	90	2448.980	2446.510	2446.695	2400.185
	365	2411.890	2412.302	2413.199	2400.897
	1000	2404.328	2406.795	2408.669	2401.874
0.1	90	244.898	244.651	246.224	241.573
	365	241.189	241.230	244.407	243.177
	1000	240.433	240.680	244.501	243.821
1.0	150	24.292	24.273	27.394	27.121
	220	24.198	24.204	27.432	27.230
	1000	24.043	24.068	27.375	27.307

The total drag coefficient is given by

$$C_D = -32B'/N_{Re}. \tag{9}$$

The results of these computations are listed as a function of N_{Re} in Table 2. The step size error was estimated from a comparison between the analytical solution and the numerical solution of the Stokes equation assuming that the inertial forces do not significantly change this error. The analysis showed that the step size error was $<0.1\%$ at low Reynolds numbers. At higher Reynolds numbers the step size was reduced until the change in the value for C_D was $<0.5\%$. The effect of the position of the outer boundary on the value of C_D was estimated from a comparison between C_D computed from our analytical solution of the Stokes equation for a bounded fluid and C_D given by the Stokes solution for an unbounded fluid, i.e.,

$$C_D = C_{Ds} = 24/N_{Re}. \tag{10}$$

The total correction, which was applied to the values of C_D obtained from the numerical solution of the nonlinear equation of motion, could therefore be found from a comparison between (10) and the numerical solution of (6). It was found that the wall correction varied with the Reynolds number. In particular, at $N_{Re}<1$ the wall effect for a given distance to the outer boundary increased strongly with decreasing N_{Re}. A similar result was found experimentally by Fidleris and Whitmore (1961). Our calculations showed that at $N_{Re}\leq 1$ the inertial terms more strongly influenced the boundary effect the greater the distance from the boundary and the smaller the Reynolds number. This is seen from Fig. 2 where the difference between C_D obtained from the numerical solution of the nonlinear and linear equations of motion is plotted as a function of $1/r_\infty$. An extrapolation of the curve for $N_{Re}=0.01$ to $1/r_\infty=0$ suggests at $1/r_\infty=0$ that $C_D=C_{Do}$, where

$$C_{Do} = \frac{24}{N_{Re}}\left(1+\tfrac{3}{16}N_{Re}\right) = C_{Ds}+4.5 \tag{11}$$

for an unbounded fluid. In a similar fashion the value of C_D corrected for an unbounded fluid was determined for $N_{Re}=0.1$ and 1.0 from Fig. 2 by graphical extrapolation.

TABLE 3. Computed values for C_D and $(D/D_s)-1$ corrected for wall effect and step size error.

N_{Re}	C_D corrected	$(D/D_s)-1$ corrected
0.01	2404.5*	1.875×10^{-3}*
0.1	244.07*	1.695×10^{-2}*
1.0	27.315*	0.1378*
5.0	7.029	0.4644
10.0	4.288	0.7867
20.0	2.711	1.2592
30.0	2.110	1.6375
40.0	1.86**	2.10**
100.0	1.12**	3.67**
100.0	1.096	3.567
200.0	0.772	5.433
300.0	0.632	6.900
400.0	0.552	8.200

* Extrapolated values (see Fig. 2).
** Adapted from Hamielec *et al.*

3. Results

The results of our investigation are displayed in Tables 3–7 and Fig. 1. In Table 3 the computed values for C_D and $(D/D_s)-1$ corrected for wall effect and step size error are listed for Reynolds numbers between 0.01 and 400. In Table 5 the corrected values for $(D/D_s)-1$ are compared with those computed from other available theoretical expressions listed in Table 4. In Table 6 the

TABLE 4. Empirical and theoretical relations for $(D/D_s)-1$.

Stokes	$(D/D_s)-1 = 0$	
Oseen	$(D/D_s)-1 = (3/16)\ N_{Re}$	
Goldstein	$(D/D_s)-1 = (3/16)\ N_{Re} - (19/1280)\ N_{Re}^2 + (71/20480)\ N_{Re}^3 - (30179/34406400)\ N_{Re}^4 + (122519/550502400)\ N_{Re}^5$	
Proudman and Pearson	$(D/D_s)-1 = (3/16)\ N_{Re} + (9/160)\ N_{Re}^2\ \ell n\ (N_{Re}/2)$	
Chester	$(D/D_s)-1 = (3/16)\ N_{Re} + (9/160)\ N_{Re}^2\ [\ell n\ (N_{Re}/2) + \gamma + (5/3)\ \ell n 2 - (323/360)] + (27/640)\ N_{Re}^3\ \ell n\ (N_{Re}/2)$; γ = Euler's constant = 0.57722	
Carrier	$(D/D_s)-1 = k_c\ (3/16)\ N_{Re}$; $k_c = 0.43$	
Pruppacher, Pruppacher and Steinberger, and Beard and Pruppacher	$(D/D_s)-1 = 0.102\ N_{Re}^{0.955}$	$0.01 \leq N_{Re} \leq 1.5$ (for minimum values)
	$(D/D_s)-1 = 0.115\ N_{Re}^{0.802}$	$3 \leq N_{Re} \leq 20$
	$(D/D_s)-1 = 0.189\ N_{Re}^{0.632}$	$20 \leq N_{Re} \leq 400$

values computed for the surface pressure and in Table 7 those for the surface vorticity are given as a function of the angle from the forward stagnation point on the sphere. Graphical comparison between the various theoretical and experimental values for $(D/D_s)-1$ is made in Fig. 1. It can be concluded from this figure that over the whole Reynolds number interval 0.01–400 the drag on a sphere calculated by the present numerical method is in close agreement with the drag obtained experimentally by Pruppacher, Pruppacher and Steinberger, and Beard and Pruppacher.

At Reynolds numbers >10 our numerical results agree closely with the numerical results of Hamielec *et al.* (1967) and those of Rimon and Cheng (1969) but

TABLE 5. Comparison of experimental and theoretically computed values for $(D/D_s)-1$.

N_{Re}		0.01	0.1	1.0	5.0	10	20	30	100	200	300	400
Present analysis (corrected values)		* $1.875X10^{-3}$	* $1.695X10^{-2}$	0.1378	0.464	0.787	1.259	1.637	3.567	5.433	6.900	8.200
Pruppacher & Steinberger	max.	$1.87\ X10^{-3}$	$1.63\ X10^{-2}$	0.115	0.418	0.729	1.271	1.622	3.471	5.379	---	---
	min.	$1.27\ X10^{-3}$	$1.14\ X10^{-2}$	0.102								
Carrier		$0.806X10^{-3}$	$0.806X10^{-2}$	0.0806	0.401	0.806	1.612	---	---	---	---	---
Oseen		$1.875X10^{-3}$	$1.875X10^{-2}$	0.1875	0.937	1.875	---	---	---	---	---	---
Goldstein		$1.874X10^{-3}$	$1.861X10^{-2}$	0.1752	0.759	1.375	---	---	---	---	---	---
Proudman & Pearson		$1.845X10^{-3}$	$1.706X10^{-2}$	0.1485	---	---	---	---	---	---	---	---

* Extrapolated values (see Fig. 2).

TABLE 6. Computed distribution of the surface pressure $P(\theta)$.

θ degrees / N_{Re}	0 96	12 108	24 120	36 132	48 144	60 156	72 168	84 180
0.01	608.583 - 55.093	595.390 -177.481	556.437 -291.481	493.453 -392.694	409.253 -476.194	307.556 -538.562	192.848 -577.105	70.174 -590.151
0.1	62.664 - 6.188	61.259 - 18.485	57.122 - 29.845	50.459 - 39.805	41.602 - 47.972	30.983 - 54.034	19.108 - 57.764	6.529 - 59.023
1.0	7.810 - 1.241	7.593 - 2.505	6.963 - 3.571	5.971 - 4.423	4.699 - 5.064	3.242 - 5.504	1.704 - 5.760	0.182 - 5.843
5.0	2.601 - 0.752	2.498 - 1.006	2.204 - 1.154	1.757 - 1.217	1.214 - 1.222	0.638 - 1.199	0.090 - 1.174	- 0.383 - 1.163
10.0	1.869 - 0.686	1.780 - 0.798	1.527 - 0.826	1.149 - 0.797	0.703 - 0.737	0.251 - 0.672	- 0.154 - 0.624	- 0.473 - 0.606
20.0	1.469 - 0.642	1.385 - 0.666	1.148 - 0.626	0.801 - 0.552	0.402 - 0.468	0.016 - 0.394	- 0.305 - 0.344	- 0.527 - 0.326
30.0	1.326 - 0.629	1.242 - 0.615	1.006 - 0.548	0.663 - 0.460	0.277 - 0.374	- 0.088 - 0.302	- 0.375 - 0.254	- 0.556 - 0.237
100.0	1.106 - 0.590	1.021 - 0.503	0.782 - 0.401	0.440 - 0.317	0.063 - 0.259	- 0.273 - 0.215	- 0.506 - 0.179	- 0.607 - 0.163
200.0	1.055 - 0.538	0.966 - 0.424	0.717 - 0.327	0.362 - 0.268	- 0.020 - 0.243	- 0.348 - 0.217	- 0.552 - 0.170	- 0.605 - 0.143
300.0	1.037 - 0.499	0.944 - 0.377	0.686 - 0.293	0.320 - 0.254	- 0.069 - 0.248	- 0.391 - 0.226	- 0.575 - 0.163	- 0.596 - 0.123
400.0	1.029 - 0.474	0.931 - 0.352	0.663 - 0.281	0.287 - 0.255	- 0.109 - 0.261	- 0.428 - 0.242	- 0.596 - 0.166	- 0.591 - 0.117

TABLE 7. Computed distribution of the surface vorticity $\zeta(\theta)$.

θ degrees / N_{Re}	0 96	12 108	24 120	36 132	48 144	60 156	72 168	84 180
0.01	0.0 1.5007	0.3151 1.4344	0.6158 1.3057	0.8894 1.1201	1.1239 0.8858	1.3090 0.6130	1.4367 0.3135	1.5015 0.0
0.1	0.0 1.5199	0.3266 1.4462	0.6375 1.3109	0.9187 1.1203	1.1574 0.8832	1.3432 0.6098	1.4681 0.3114	1.5276 0.0
1.0	0.0 1.672	0.4229 1.5352	0.8182 1.3435	1.1623 1.1114	1.4358 0.8518	1.6259 0.5754	1.7268 0.2897	1.7397 0.0
5.0	0.0 2.0534	0.7064 1.7229	1.3489 1.3634	1.8738 1.0130	2.2418 0.6978	2.4330 0.4289	2.4487 0.2020	2.3101 0.0
10.0	0.0 2.3894	0.9676 1.8871	1.8373 1.3842	2.5276 0.9363	2.9800 0.5766	3.168 0.3139	3.1005 0.1332	2.8191 0.0
20.0	0.0 2.8121	1.3710 2.0422	2.5904 1.3327	3.5316 0.7604	4.1045 0.3581	4.2711 0.1227	4.0524 0.0224	3.5265 0.0
30.0	0.0 3.1042	1.7012 2.1145	3.2063 1.2482	4.3514 0.5938	5.0189 0.1737	5.1596 - 0.0316	4.8043 - 0.0658	4.0629 0.0
100.0	0.0 4.0104	3.2065 1.9723	6.0259 0.5340	8.1233 - 0.2569	9.2405 - 0.6192	9.2415 - 0.7443	8.1625 - 0.5479	6.2604 0.0
200.0	0.0 4.1712	4.6589 1.2851	8.7359 - 0.2794	11.7232 - 0.7631	13.2173 - 0.9827	12.9818 - 1.5876	11.0355 - 1.4593	7.7948 0.0
300.0	0.0 3.9009	5.8176 0.5710	10.8874 - 0.7932	14.5566 - 0.8289	16.3027 - 1.2406	15.8046 - 2.7085	13.0588 - 2.5656	8.6295 0.0
400.0	0.0 3.4658	6.8352 -0.0438	12.7666 - 1.0929	17.0087 - 0.6858	18.9346 - 1.5462	18.1513 - 3.8480	14.6377 - 3.6228	9.1099 0.0

depart significantly from the results of Jenson (1959) whose rather large step sizes used in his numerical computations may have biased his results. The variation of our computed values for the drag with Reynolds number suggests that as the Reynolds number approaches zero the drag approaches zero via the Oseen drag as originally suggested experimentally by Maxworthy, and Pruppacher and Steinberger. Fig. 1 further suggests that the theories of Oseen, Goldstein, and Proudman and Pearson are only applicable at $N_{Re} \lesssim 0.1$. At larger Reynolds numbers these theories progressively overestimate the drag. At intermediate Reynolds numbers ($2 \leq N_{Re} < 20$), the theoretical considerations of Carrier approximate our numerical and experimental results better than any other theory. At $N_{Re} > 20$ a determination of the drag and flow fields must rely on numerical methods.

Acknowledgments. Two of the authors (B. P. L. C., A. E. H.) are indebted to the National Research Council of Canada and the other (H. R. P.), to the National Science Foundation under Grant No. GA-759 for supporting the research reported in this paper.

APPENDIX

Nomenclature

A	lattice spacing in radial direction
a	radius of sphere
B	lattice spacing in angular direction
A', B', C', D'	constants in Eq. (7)
C_D	total drag coefficient (form drag plus friction drag)
C_{Do}	total drag force coefficient in Oseen type flow
C_{Ds}	total drag force coefficient in Stokes type flow
D	drag force on a sphere at terminal velocity, i.e., net gravitational force on sphere, $(4/3)\pi a^3(\rho_s - \rho_m)g$
D_s	viscous drag force in Stokes flow regime, $6\pi\mu a V_\infty$
L^2	differential operator
g	acceleration of gravity
N_{Re}	Reynolds number, $2aV_\infty/\nu$
P_0	dimensionless frontal stagnation pressure, $(P_0' - P_\infty')/(\frac{1}{2}\rho_m V_\infty^2)$
P_π	dimensionless rear stagnation pressure, $(P_\pi' - P_\infty')/(\frac{1}{2}\rho_m V_\infty^2)$
$P(\theta)$	dimensionless pressure at surface of sphere, $[P'(\theta) - P_\infty']/(\frac{1}{2}\rho_m V_\infty^2)$
P_∞'	static pressure in undisturbed fluid medium
r	dimensionless radial coordinate, r'/a
r_∞	dimensionless radial distance to outer boundary, r_∞'/a
v_θ, v_r	dimensionless angular and radial velocity, v_θ'/V_∞, v_r'/V_∞, respectively
V_∞	terminal velocity of sphere
W, V	relaxation factors
θ	angular spherical coordinate (angle from forward stagnation point)
ψ	dimensionless stream function, $\psi'/(V_\infty a^2)$
μ, ν	dynamic and kinematic viscosity, respectively
ρ_m, ρ_s	fluid and sphere density, respectively
ζ	dimensionless vorticity, $\zeta' a/V_\infty$

REFERENCES

Beard, K., and H. R. Pruppacher, 1969: A determination of the terminal velocity and drag of small water drops by means of a wind tunnel. *J. Atmos Sci.*, **26**, 1066–1072.

Carrier, G. F., 1953: On slow viscous flow. Office of Naval Research, Final Rept., Contract Nonr-653–00/1, 31 pp.

Chester, W., and D. R. Breach, 1969: On the flow past a sphere at low Reynolds numbers. *J. Fluid Mech.*, **37**, 751–760.

Davis, M. H., 1966: Collisions of very small cloud drops. *J. Geophys. Res.*, **71**, 3101–3104.

——, and D. Sartor, 1967: Theoretical collision efficiencies for small cloud droplets in Stokes flow. *Nature*, **215**, 1371–1372.

Fidleris, V., and R. L. Whitmore, 1961: Experimental determination of the wall effect for spheres falling axially in cylindrical vessels. *Brit. J. Appl. Phys.*, **12**, 490–494.

Goldstein, S., 1929: The forces on a solid body moving through viscous fluid. *Proc. Roy. Soc. London*, **A123**, 216–235.

Hamielec, A. E., T. W. Hoffmann and L. L. Ross, 1967: Numerical solution of the Navier Strokes equations for flow past spheres. *A.I.Ch.E. J.*, **13**, 212–219.

Hocking, L. M., 1959: The collision efficiency of small drops. *Quart. J. Roy. Meteor. Soc.*, **85**, 44–50.

Jenson, V. G., 1959: Viscous flow round a sphere at low Reynolds numbers. *Proc. Roy. Soc. London*, **A249**, 346–366.

Klett, J., 1969: The interaction and motion of rigid spheres falling in a viscous fluid at low Reynolds numbers. Ph.D. thesis, University of California, Dept. of Meteorology, Los Angeles.

Langmuir, I., 1948: The production of rain by a chain reaction in cumulus clouds at temperatures above freezing. *J. Meteor.*, **5**, 157–192.

Maxworthy, T., 1965: Accurate measurements of sphere drag at low Reynolds numbers. *J. Fluid Mech.*, **23**, 369–372.

Oseen, C. W., 1927: *Hydrodynamik*. Akad. Leipzig, Verlagsgesellschaft, 337 pp.

Pearcey, T., and G. W. Hill, 1957: A theoretical estimate of the collection efficiencies of small droplets. *Quart. J. Roy. Meteor. Soc.*, **83**, 77–93.

Plumlee, H. R., and R. G. Semonin, 1965: Cloud droplet collision efficiency in electric fields. *Tellus*, **17**, 356–363.

Proudman, I., and J. R. A. Pearson, 1957: Expansions at small Reynolds numbers for the flow past a sphere and a circular cylinder. *J. Fluid Mech.*, **2**, 237–262.

Pruppacher, H. R., and E. H. Steinberger, 1968: An experimental determination of the drag on a sphere at low Reynolds numbers. *J. Appl. Phys.*, **39**, 4129–4132.

Rimon, Y., and S. I. Cheng, 1969: Numerical solution of a uniform flow over a sphere at intermediate Reynolds numbers. *Phys. Fluids*, **12**, 949–959.

Shafrir, U., and M. Neiburger, 1963: Collision efficiencies of two spheres falling in a viscous medium. *J. Geophys. Res.*, **68**, 4141–4147.

Steinberger, E. H., H. R. Pruppacher and M. Neiburger, 1968: On the hydrodynamics of pairs of spheres falling along their line of centers in a viscous medium. *J. Fluid Mech.*, **34**, 809–819.